Parameter Sensitivities of the Dual-Localization Approach in the Local Ensemble Transform Kalman Filter

Keiichi Kondo[1,2], Takemasa Miyoshi[2,3,4] and H. L. Tanaka[5]

[1]*Graduate School of Life and Environmental Sciences*, *University of Tsukuba, Tsukuba, Japan*
[2]*RIKEN Advanced Institute for Computational Science, Kobe, Japan*
[3]*University of Maryland, College Park, Maryland, USA*
[4]*Earth Simulator Center, Japan Agency for Marine-Earth Science and Technology, Yokohama, Japan*
[5]*Center for Computational Sciences, University of Tsukuba, Tsukuba, Japan*

Abstract

In the ensemble Kalman filter, covariance localization plays an essential role in treating sampling errors in the ensemble-based error covariance between distant locations. We may limit the influence of observations excessively, particularly when the model resolution is very high, since larger-scale structures than the localization scale are removed due to tight localization for the high-resolution model. To retain the larger-scale structures with a limited ensemble size, the dual-localization approach, which considers two separate localization scales simultaneously, has been proposed. The dual-localization method analyzes small-scale and large-scale analysis increments separately using spatial smoothing and two localization scales. These are the control parameters of the dual-localization method, and this study aims to investigate the parameter sensitivities by performing a number of observing system simulation experiments using an intermediate AGCM known as the SPEEDY model. Two smoothing functions, the spherical harmonics spectral truncation and the Lanczos filter, are tested, and the results indicate no significant difference. Also, sensitivity to the two localization parameters is investigated, and the results show that the dual-localization approach outperforms traditional single localization with relatively wide choices of the two localization scales by about 400-km ranges. This suggests that we could avoid fine tuning of the two localization parameters.

(**Citation:** Kondo, K., T. Miyoshi, and H. L. Tanaka, 2013: Parameter sensitivities of the dual-localization approach in the local ensemble transform kalman filter. *SOLA*, **9**, 174−178, doi: 10.2151/sola.2013-039.)

1. Introduction

Data assimilation generates accurate initial conditions by extracting the most information from both model forecasts and observations. Numerical weather prediction (NWP) is generally sensitive to the initial conditions, and it is essential to obtain better initial conditions using more advanced data assimilation methods. The ensemble Kalman filter (EnKF; Evensen 1994) is an advanced data assimilation method, and a number of research articles on EnKF have been published so far. Various EnKF approaches have been suggested, such as the Ensemble Adjustment Kalman Filter (EAKF, Anderson 2001), Serial Ensemble Square Root Filter (Whitaker and Hamill 2002), Ensemble Transform Kalman Filter (ETKF; Bishop et al. 2001), and Local Ensemble Kalman Filter (LEKF; Ott et al. 2004). Hunt et al. (2007) suggested the Local Ensemble Transform Kalman Filter (LETKF) by applying the ETKF algorithm to the LEKF. Miyoshi and Yamane (2007) applied the LETKF to the Earth Simulator global model known as the AFES (Atmospheric General Circulation Model for the Earth Simulator; Ohfuchi et al. 2004), and investigated its performance in detail. Recently, a growing number of LETKF studies have been published. Kondo and Tanaka (2009) applied the LETKF to the NICAM (Nonhydrostatic Icosahedral Atmospheric Model) which is particularly designed for global cloud-resolving simulations by directly calculating cloud physics in the global domain (Satoh et al. 2008). Kalnay and Yang (2010) proposed and tested the RIP (Running-In-Place) approach with the LETKF to accelerate the spin-up time. Miyoshi and Kunii (2012) applied the LETKF to the WRF (Weather Research and Forecasting; Skamarock et al. 2005) model.

When we apply EnKF to realistic meteorological problems, localization (Houtekamer and Mitchell 1998; Hamill et al. 2001) plays an essential role in dealing with spurious sampling errors due to a generally limited ensemble size. EnKF is generally unstable without localization mainly because of sampling errors between distant locations. Localization limits the impact of observations within a certain distance defined by a prescribed localization function. The localization function is usually a distance-dependent function that drops to zero at a certain distance, and the Gaspari and Cohn (1999)'s fifth-order polynomial function is a typical choice. The optimal localization scale depends on several factors including the model resolution and ensemble size; the localization scale becomes generally smaller for higher-resolution models. For example, Miyoshi et al. (2010) applied the 400-km localization scale for a T319/L40 (horizontal resolution up to 319 wave-numbers and 40 vertical levels) global model, and Miyoshi et al. (2007) applied the 500-km localization scale for the T159/L48 AFES. By contrast, for the T30/L7 SPEEDY model (Molteni 2003) the optimal localization scale is found to be 700 km (Kang, personal communication). In mesoscale model, Zhang et al. (2009) applied about 340-km, 120-km and 40-km localization scale for the WRF model whose corresponding horizontal resolutions are 40.5 km, 13.5 km and 4.5 km, respectively. If we have a very high-resolution mesoscale model with a 1-km or even finer grid spacing, the localization scale would likely be limited up to $O(10)$-km. In fact, Yussouf and Stensrud (2010) applied an approximately 1.1-km localization scale (4-km radius of influence) with 1-km horizontal resolution model for radar data assimilation. In such cases, observations are used only in such limited distance, although at least some observations such as rawinsondes are expected to observe synoptic-scale weather with at least $O(100)$-km scale. Therefore, if we apply narrow localization up to $O(10)$-km for high resolution models, EnKF may not account for larger-scale errors even though the observations shall provide useful information at $O(100)$-km scale.

Multi-scale consideration is essential to tackle these situations and to use precious observations more effectively. Buehner (2012) proposed a spatial and spectral covariance localization approach, which considers separate scales simultaneously. This way, we can account for larger-scale error covariances separately from smaller-scale error covariances. Larger-scale error covariances are expected to have larger-scale structure, which usually requires large-scale localization. This enables longer-distance impact from observations even if the model resolution is high. The separate consideration of higher-resolution error covariances allows simul-

taneous analysis of fine structure near the observations. Inspired by Buehner (2012), Miyoshi and Kondo (2013) proposed the dual-localization approach that considers two localization scales simultaneously. In the dual-localization method, longer-range analysis increments are analyzed by applying a spatial smoothing to the ensemble perturbations and using a larger localization scale, while simultaneously, shorter-range analysis increments are analyzed by using a smaller localization scale. Here, the smoothing function and two localization scales are the control parameters of the dual-localization approach. Miyoshi and Kondo (2013) did not investigate the parameter sensitivities, which are the focus of this study.

To make this paper self-contained, Section 2 provides a brief overview of the dual-localization approach. Section 3 describes the experimental design, and the results are presented in Section 4. Finally, conclusion is provided in Section 5.

2. Dual-localization method

The essence of the dual-localization approach is to find the analysis increments as a sum of the small-scale and large-scale components. The full-resolution ensemble perturbations and the reduced-resolution ensemble perturbations obtained by smoothing the full-resolution perturbations are combined with small-scale and large-scale localizations, respectively. In this paper the method is derived based on the LETKF, but the same idea may be applied to other EnKF implementations in a straightforward manner.

The smaller-scale, high-resolution component $\delta\mathbf{X}_h$ is obtained by the full-resolution forecast ensemble perturbations with a short-range localization scale (Fig. 1 a, with 500-km localization). The subscript h represents using high-resolution perturbations. In the LETKF, $\delta\mathbf{X}_h$ is given by

$$\delta\mathbf{X}_h = \delta\mathbf{X}^f\tilde{\mathbf{P}}^a(\mathbf{H}\delta\mathbf{X}^f)^T(\tilde{\rho}_{short}\circ\mathbf{R}^{-1})(\mathbf{y}^o - \mathbf{H}\bar{\mathbf{x}}^f) \\ + \delta\mathbf{X}^f[(N-1)\tilde{\mathbf{P}}^a]^{1/2}, \tag{1}$$

where $\circ$ denotes the element-wise multiplication. Each column of the background ensemble perturbation matrix $\delta\mathbf{X}^f$ is composed of the difference between each ensemble forecast and the ensemble mean $\bar{\mathbf{x}}^f$, and the ensemble size is N. $\tilde{\mathbf{P}}^a$, $\mathbf{H}$, $\mathbf{R}$ and $\mathbf{y}^o$ denote the analysis error covariance in ensemble space, the linear tangent matrix of the observation operator, observation error covariance matrix (assumed to be diagonal) and observation vector, respectively. In the LETKF we apply observation localization $\tilde{\rho}_{short}$ to $\mathbf{R}^{-1}$ and weigh the observation error variances depending on the distance from the analyzed grid point (Hunt et al. 2007; Miyoshi and Yamane 2007; Greybush et al. 2011).

The larger-scale, low-resolution component $\delta\mathbf{X}_l$ is computed from reduced-resolution forecast ensemble perturbations with a longer-range localization scale. $\delta\mathbf{X}_l$ is composed of $\delta\mathbf{X}_{l-long}$ and $\delta\mathbf{X}_{l-short}$. The subscript l represents low-resolution perturbations, followed by *long* (*short*) denoting a long-range (short-range) localization scale. $\delta\mathbf{X}_{l-long}$ (Fig. 1b) is obtained from $\delta\mathbf{X}_l^f$ with longer-range localization:

$$\delta\mathbf{X}_{l-long} = \delta\mathbf{X}_l^f\tilde{\mathbf{P}}_{l-long}^a(\mathbf{H}\delta\mathbf{X}_l^f)^T(\tilde{\rho}_{long}\circ\mathbf{R}^{-1})(\mathbf{y}^o - \mathbf{H}\bar{\mathbf{x}}^f) \\ + \delta\mathbf{X}_l^f[(N-1)\tilde{\mathbf{P}}_{l-long}^a]^{1/2}, \tag{2}$$

where the localization scale of $\tilde{\rho}_{long}$ is longer than that of $\tilde{\rho}_{short}$. Although $\delta\mathbf{X}_l^f$ is obtained by applying a spatial low-pass filter (i.e., spatial smoothing) to $\delta\mathbf{X}^f$, $\bar{\mathbf{x}}^f$ is not smoothed and is the same as that in (1). $\delta\mathbf{X}_{l-long}$ includes a short-range structure $\delta\mathbf{X}_{l-short}$, which needs to be removed. $\delta\mathbf{X}_{l-short}$ is obtained from $\delta\mathbf{X}_l^f$ with smaller localization scale:

$$\delta\mathbf{X}_{l-short} = \delta\mathbf{X}_l^f\tilde{\mathbf{P}}_{l-short}^a(\mathbf{H}\delta\mathbf{X}_l^f)^T(\tilde{\rho}_{short}\circ\mathbf{R}^{-1})(\mathbf{y}^o - \mathbf{H}\bar{\mathbf{x}}^f) \\ + \delta\mathbf{X}_l^f[(N-1)\tilde{\mathbf{P}}_{l-short}^a]^{1/2}, \tag{3}$$

where $\tilde{\rho}_{short}$ is the same as that in (1).

The resulting multi-scale increment $\delta\mathbf{X}$ is obtained form (1), (2) and (3) and is shown in Fig. 1c. $\delta\mathbf{X}$ is computed by

$$\delta\mathbf{X} = \delta\mathbf{X}_h + \delta\mathbf{X}_{l-long} - \delta\mathbf{X}_{l-short}. \tag{4}$$

$\delta\mathbf{X}_h$ provides the short-range, small-scale structure, and $\delta\mathbf{X}_l = \delta\mathbf{X}_{l-long} - \delta\mathbf{X}_{l-short}$ provides the long-range, large-scale structure. If the long and short localization scales are the same, the dual-localization approach reduces to the single localization approach. Although the dual-localization approach requires solving the LETKF analysis updates three times, usually that is not a large load since the major part of LETKF computations is usually in the ensemble forecasting part, which remains the same.

Miyoshi and Kondo (2013) obtained the smoothed ensemble perturbations $\delta\mathbf{X}_l^f$ by applying the spectral truncation in the spherical harmonics. In this study, we apply the Lanczos filter (Lanczos 1956; Duchon 1979). The Lanczos filter has two parameters: resolution parameter n and critical frequency f_c. In this study, n is chosen to be 10, and f_c is selected from 1/5, 1/8 and 1/11. The Lanczos filter is applied to the longitude and latitude directions. Figure 2 shows the response functions of the Lanczos filter and Fourier transform. The curve of Fourier transform is an ideal response function with cut-off wave number 21. The three curves of Lanczos filters are the smoothed response function with transition bands. The smaller f_c corresponds to more smoothing. The traditional single localization approach and the dual-localization approach are called "CTRL" and "DLOC", respectively, and sometimes subscript F or L is added, corresponding to the Fourier transform (F) and Lanczos filter (L), respectively. Figure 3 illus-
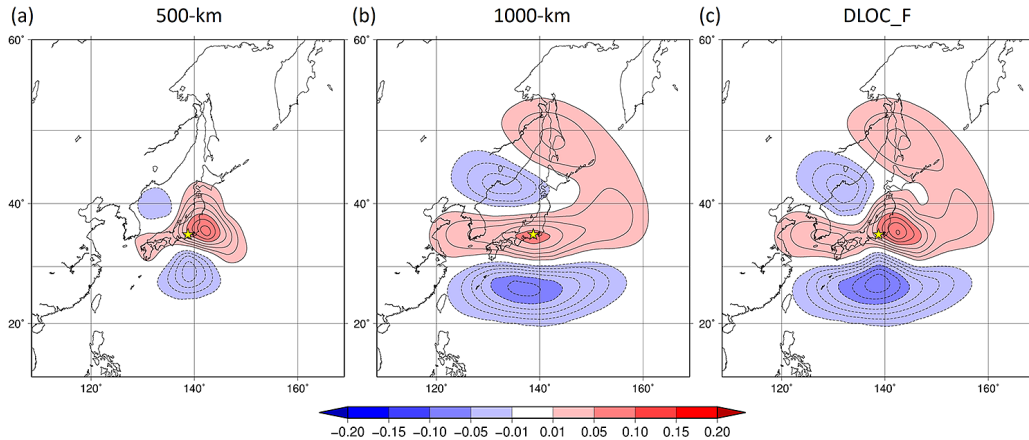

Fig. 1. Analysis increments of zonal wind (m s^{-1}) at the 4th model level (~500 hPa) from a single profile observation at the star point using the SPEEDY model using (a) full-resolution ensemble perturbations with 500-km localization, (b) smoothed ensemble perturbations with 1000-km localization (T21 spectral truncation), and (c) dual localization with 500-km and 1000-km localization scales using T21 spectral truncation for spatial smoothing. These figures are adopted from Figs. 1b, 2b and 4 of Miyoshi and Kondo (2013).
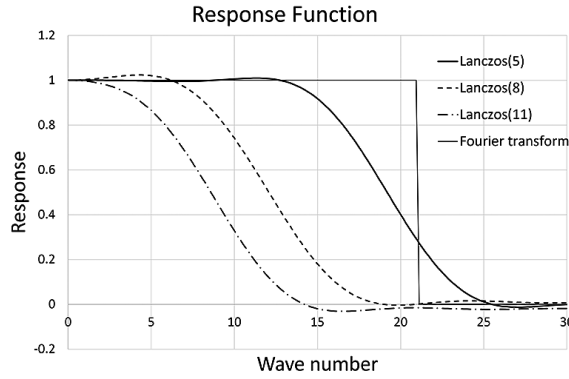
Fig. 2. Response functions of the Fourier transform (thin solid) and the Lanczos filters with f_c = 1/5 (thick solid), 1/8 (dashed) and 1/11 (dash-dotted).

trates similar analysis increments as Fig. 1c, but with the Lanczos filter. If we choose a stronger smoothing parameter, $\delta \mathbf{X}_l$ becomes smaller and smaller by cancelling out positive and negative values, and the analysis increments become similar to those with single 500-km localization $\delta \mathbf{X}_h$ (Figs. 1a and 3c). This study compares the analysis accuracy among different smoothing functions.

3. Experimental settings

In this study, twin experiments with a T30/L7 (horizontal resolution up to 30 wave numbers and 7 vertical levels) atmospheric general circulation model (AGCM) known as the SPEEDY model (Molteni 2003) are performed under the perfect model scenario. This type of experiments is also known as the OSSE (observing system simulation experiment). The horizontal resolution of the SPEEDY model is about 420 km (3.75 degrees in longitude), and the prognostic variables are zonal and meridional wind components (U, V), temperature (T), specific humidity (Q) and surface pressure (Ps).

The experimental settings follow Miyoshi and Kondo (2013). Namely, the nature run starts at 0000 UTC 1 January 1982, and the observations are generated by adding uncorrelated white random numbers to the nature run. The observation error standard deviations are 1.0 m s^{-1} for U and V, 1.0 K for T, 1.0 × 10^{-3} kg kg^{-1} for Q and 1.0 hPa for Ps. The observations are taken every 6 hours at all 7 vertical levels at given horizontal stations of a radiosonde-like network, but the observations of specific humidity and surface pressure are taken from the bottom to the 4th level and only at the surface, respectively. The assimilation

cycle is every 6 hour, and the period of the experiments is from 0000 UTC 1 January 1982 to 0000 UTC 1 February 1983. The ensemble size is fixed at 20, and the initial ensemble members are chosen from the nature run in January 1984. All experiments are performed with adaptive covariance inflation (Miyoshi 2011). The CTRL experiment employs the traditional LETKF with 700-km horizontal and 0.1 ln p vertical localization parameters. The other experiments employ the dual-localization approach (DLOC) with different choices of smoothing functions and localization parameters. DLOC_F uses the spectral truncation at 21 wavenumbers, and DLOC_L5 uses Lanczos filter with f_c = 1/5, and similarly to DLOC_L8 and DLOC_L11. The localization parameters are chosen by 100-km increment from 300 km to 900 km for the short localization, and from 600 km to 1300 km for the long localization. By definition, the long localization parameter is always greater than the short localization parameter.

4. Results

Figure 4 illustrates the results of the localization parameter survey for different choices of the smoothing functions. Figure 4 indicates RMSE (Root Mean Square Error) of surface pressure, and the shaded area corresponds to the advantage of DLOC over CTRL. DLOC_F and DLOC_L5 are very similar (Figs. 4a, b), and the smallest RMSE values are almost identical. Figures 4b, c, d show the impact of the smoothing strength. As the degree of smoothing becomes stronger, the optimal localization parameters shifts to larger scales, and the shaded area becomes smaller. The smallest RMSE in Fig. 4c is almost the same as that of Fig. 4b, but Fig. 4d shows larger RMSE. Hereafter, DLOC_L5 is further investigated and is denoted simply as DLOC_L.

Figure 5 is similar to Fig. 4, but for zonal wind, temperature and specific humidity. DLOC_L outperforms CTRL with relatively wide choices of the two localization parameters by about 400-km range, that is, 400−900 km for the short localization parameter and 700−1100 km for the long localization parameter. Using the longer localization parameter greater than 1200 km causes filter divergence. U and Ps (Fig. 4b) show a little more sensitivity to the localization parameters than T and Q. The shapes of shaded area are similar except for Q. The positions of minimum RMSE differ among different variables. Figures 4 and 5 suggest that the best combination of short and long localization parameters be 600 km and 900 km. A similar localization parameter survey is performed for DLOC_F, and the optimal localization parameters are found to be 500 km and 900 km (not shown).

Figure 6 shows the horizontal power spectrums of the analysis error of zonal wind at the 4th model level (~500 hPa). Here, the optimal localization parameters are chosen. The analysis errors are computed from the difference between the nature run and analysis, and has the most power around the horizontal wave
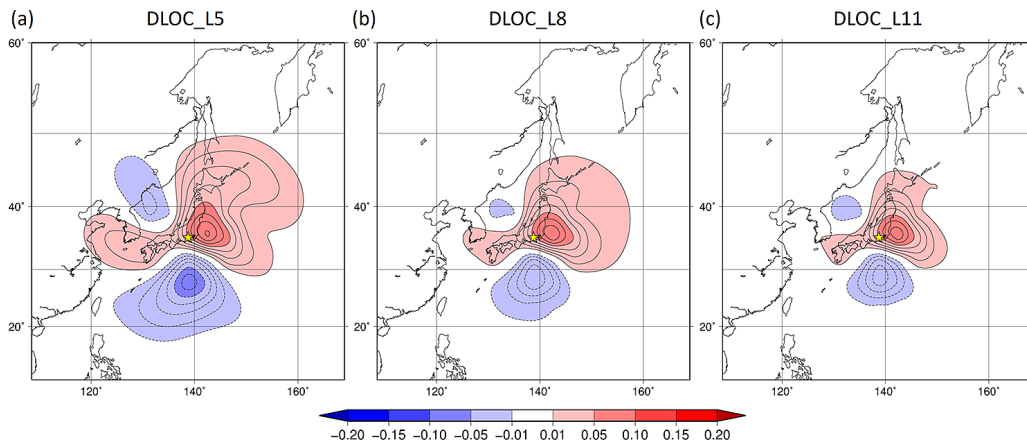

Fig. 3. Similar to Fig. 1c, but using the Lanczos filter with f_c = (a) 1/5, (b) 1/8 and (c) 1/11.

numbers 10 to 20. By applying the dual-localization approach, the analysis errors become much smaller in all wavenumbers, and the improvement was about 20%. There is no significant difference between DLOC_F and DLOC_L.
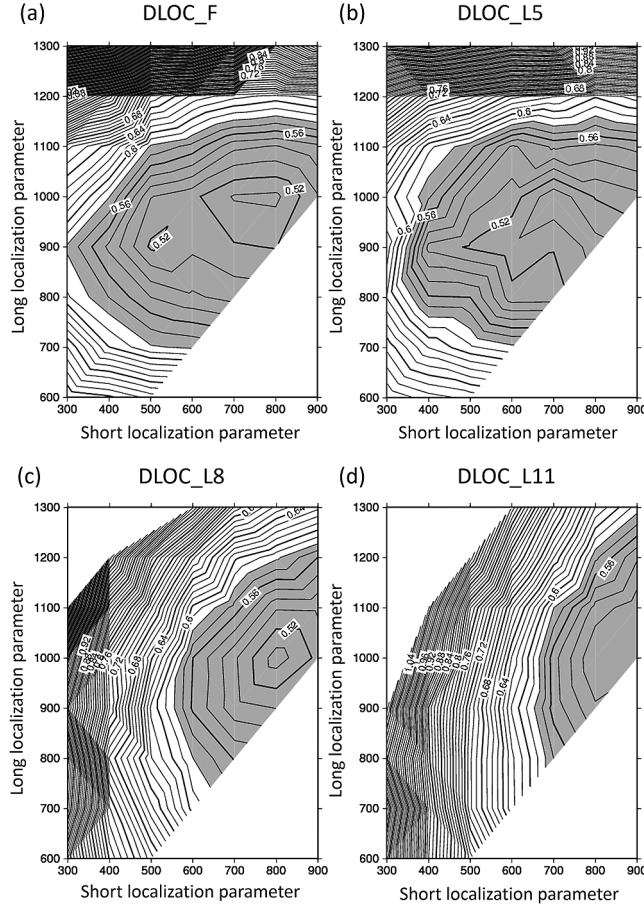
5. Conclusion

The dual-localization approach of Miyoshi and Kondo (2013) analyzes the high-resolution and low-resolution components of analysis increments separately, using two localization scales and spatial smoothing. The two localization scale parameters and the choice of the smoothing function are the tuning parameters of the dual-localization method. This study aims to investigate the parameter sensitivities. The results showed robust performance of the dual-localization approach. Namely, dual localization (DLOC) outperformed traditional single localization (CTRL) with a relatively wide choices of the two localization scale parameters by about 400-km range. Also, two smoothing functions, the spectral truncation as in Miyoshi and Kondo (2013) and the Lanczos filter, gave essentially identical analysis performance if their smoothing strengths are similar. These findings are important in the sense that we may avoid a fine tuning of the parameters of dual localization. Since the Lanczos filter is simpler to implement and faster to compute, the Lanczos filter may be advantageous in implementing with higher-resolution regional models. Results also showed that the performance of the dual-localization approach strongly depends on the smoothing strength. With stronger smoothing, larger localization parameters give better results, although the minimum RMSE becomes slightly larger with stronger smoothing. Testing the dual-localization approach with real observations and more realistic models remains a subject of future research.

Fig. 4. Analysis RMSEs of surface pressure (hPa) of dual localization with various localization scale parameters, averaged for a year from 0000 UTC 1 February 1982 to 0000 UTC 1 February 1983, and using (a) T21 spectral truncation, (b) Lanczos filter with $f_c = 1/5$, (c) $f_c = 1/8$ and (d) $f_c = 1/11$. The shaded areas indicate improvements of DLOC over CTRL whose RMSE is 0.586 hPa.
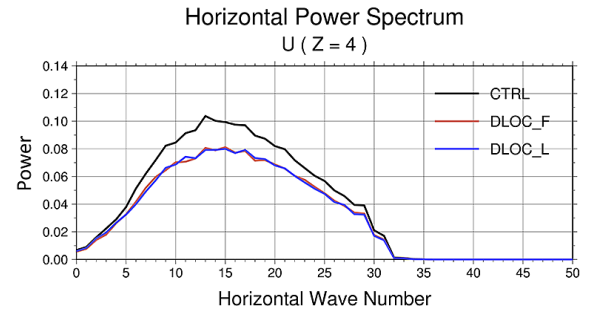

Fig. 6. Horizontal power spectrum of the zonal wind analysis errors at the 4th model level for CTRL (black), DLOC_F (red) and DLOC_L (blue).
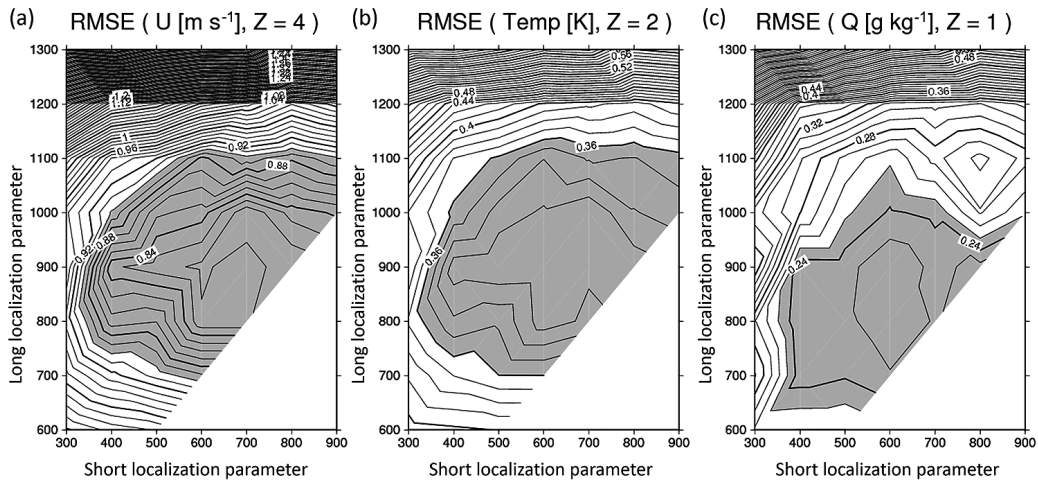

Fig. 5. Similar to Fig. 4b, but for (a) zonal wind (m s^{-1}) at the 4th model level, (b) temperature (K) at the second model level and (c) specific humidity (g kg^{-1}) at the lowest model level. The RMSEs of CTRL are 0.900 m s^{-1}, 0.366 K and 0.258 g kg^{-1}, respectively.

Acknowledgements

References

Anderson, J. L., 2001: An ensemble adjustment Kalman filter for data assimilation. *Mon. Wea. Rev.*, **129**, 2884−2903.

Bishop, C. H., B. J. Etherton, and S. J. Majumdar, 2001: Adaptive sampling with the ensemble transform Kalman filter. Part I: Theoretical aspects. *Mon. Wea. Rev.*, **129**, 420−436.

Buehner, M., 2012: Evaluation of a spatial/spectral covariance localization approach for atmospheric data assimilation. *Mon. Wea. Rev.*, **140**, 617−636.

Duchon, C. E., 1979: Lanczos filtering in one and two dimensions. *J. Appl. Meteor.*, **18**, 1016−1022.

Evensen, G., 1994: Sequential data assimilation with a nonlinear quasi-geostrophic model using Monte Carlo methods to forecast error statistics. *J. Geophys. Res.*, **99C5**, 10143−10162.

Gaspari, G., and S. E. Cohn, 1999: Construction of correlation functions in two and three dimensions. *Quart. J. Roy. Meteor. Soc.*, **125**, 723−757.

Greybush, S. J., E. Kalnay, T. Miyoshi, K. Ide, and B. R. Hunt, 2011: Balance and ensemble Kalman filter localization techniques. *Mon. Wea. Rev.*, **139**, 511−522.

Hamill, T. M., J. Whitakaer, and C. Snyder, 2001: Distance-dependent filtering of background error covariance estimates in an ensemble Kalman filter. *Mon. Wea. Rev.*, **129**, 2776−2790.

Houtekamer, P. L., and H. L. Mitchell, 1998: Data assimilation using an ensemble Kalman filter Technique. *Mon. Wea. Rev.*, **126**, 796−811.

Hunt, B. R., E. Kostelich, and I. Syzunogh, 2007: Efficient data assimilation for spatiotemporal chaos: A local ensemble transform Kalman filter. *Physica D*, **230**, 112−126.

Kalnay, E., and S.-C. Yang, 2010: Accelerating the spin-up of ensemble Kalman filtering. *Quart. J. Roy. Meteor. Soc.*, **136**, 1644−1651.

Kondo, K., and H. L. Tanaka, 2009: Applying the local ensemble transform Kalman filter to the nonhydrostatic icosahedral atmospheric model (NICAM). *SOLA*, **5**, 121−124.

Lanczos, C., 1956: *Applied Analysis*. Prentice-Hall, 539 pp.

Miyoshi, T., 2011: The Gaussian approach to adaptive covariance inflation and its implementation with the local ensemble transform Kalman filter. *Mon. Wea. Rev.*, **139**, 1519−1535, doi:10.1175/2010MWR3570.1.

Miyoshi, T., and S. Yamane, 2007: Local ensemble transform Kalman filtering with an AGCM at a T159/L48 Resolution. *Mon. Wea. Rev.*, **135**, 3841−3861.

Miyoshi, T., and M. Kunii, 2012: The local ensemble transform Kalman filter with the Weather Research and Forecasting model: Experiments with real observations. *Mon. Wea. Rev.*, **169**, 321−333.

Miyoshi, T., and K. Kondo, 2013: A multi-scale localization approach to an ensemble Kalman filter. *SOLA*, **9**, 170−173.

Miyoshi, T., S. Yamane, and T. Enomoto, 2007: Localizing the error covariance by physical distances within a local ensemble transform Kalman filter (LETKF). *SOLA*, **3**, 89−92.

Miyoshi, T., Y. Sato, and T. Kadowaki, 2010: Ensemble Kalman filter and 4D-Var intercomparison with the japanese operational global analysis and prediction system. *Mon. Wea. Rev.*, **138**, 2846−2866.

Molteni, F., 2003: Atmospheric simulations using a GCM with simplified physical parametrizations. I: model climatology and variability in multi-decadal experiments. *Clim. Dyn.*, **20**, 175−191.

Ohfuchi, W., H. Nakamura, M. K. Yoshioka, T. Enomoto, K. Takaya, X. Peng, S. Yamane, T. Nishimura, Y. Kurihara, and K. Ninomiya, 2004: 10-km mesh mesoscale resolving simulations of the global atmosphere on the Earth Simulator: Preliminary outcomes of AFES (AGCM for the Earth Simulator). *J. Earth Simulator*, **1**, 8−34.

Ott, E., and co-authors, 2004: A local ensemble Kalman filter for atmospheric data assimilation. *Tellus*, **56A**, 415−428.

Satoh, M., T. Matsuno, T. H. Tomita, H. Miura, T. Nasuno, S. Iga, 2008: Nonhydrostatic Icosahedral Atmospheric Model (NICAM) for global cloud resolving simulations. *Journal of Computational Physics*, the special issue on Predicting Weather, Climate and Extreme events, **227**, 3486−3514, doi:10.1016/j.jcp.2007.02.006.

Skamarock, W. C., J. B. Klemp, J. Dudhia, D. O. Gill, D. M. Barker, W. Wang, and J. G. Powers, 2005: *A description of the Advanced Research WRF* version 2. NCAR Tech. Note TN- 468 + STR, 88 pp.

Whitaker, J. S., and T. M. Hamill, 2002: Ensemble data assimilation without perturbed observations. *Mon. Wea. Rev.*, **130**, 1913−1924.

Yussouf, N., and D. J. Stensrud, 2010: Impact of phased-array radar observations over a short assimilation period: Observing system simulation experiments using an ensemble Kalman filter. *Mon. Wea. Rev.*, **138**, 517−538.

Zhang, F., Y. Weng, J. A. Sippel, Z. Meng, and C. H. Bishop, 2009: Cloud-Resolving hurricane Initialization and prediction through assimilation of doppler radar observations with an ensemble Kalman filter. *Mon. Wea. Rev.*, **137**, 2105−2125.